

VM-UNET-V2: Rethinking Vision Mamba UNet for Medical Image Segmentation

Mingya Zhang¹ and Yue Yu² Limei Gu³ Tingsheng Lin³ and Xianping Tao¹

¹ State Key Laboratory for Novel Software Technology, Nanjing University
dg20330034@smail.nju.edu.cn

² Huazhong University of Science and Technology

³ Jiangsu Province Hospital of Chinese Medicine

Abstract. In the field of medical image segmentation, models based on both CNN and Transformer have been thoroughly investigated. However, CNNs have limited modeling capabilities for long-range dependencies, making it challenging to exploit the semantic information within images fully. On the other hand, the quadratic computational complexity poses a challenge for Transformers. Recently, State Space Models (SSMs), such as Mamba, have been recognized as a promising method. They not only demonstrate superior performance in modeling long-range interactions, but also preserve a linear computational complexity. Inspired by the Mamba architecture, We proposed Vision Mamba-UNetV2, the Visual State Space (VSS) Block is introduced to capture extensive contextual information, the Semantics and Detail Infusion (SDI) is introduced to augment the infusion of low-level and high-level features. We conduct comprehensive experiments on the ISIC17, ISIC18, CVC-300, CVC-ClinicDB, Kvasir, CVC-ColonDB and ETIS-LaribPolypDB public datasets. The results indicate that VM-UNetV2 exhibits competitive performance in medical image segmentation tasks. Our code is available at <https://github.com/nobodyplayer1/VM-UNetV2>.

Keywords: Medical Image Segmentation · UNet · Vision State Space Models

1 Introduction

As medical imaging technology continues to advance, medical images have become a crucial tool for diagnosing diseases and planning treatments [6]. Among the fundamental and critical techniques in medical image analysis, medical image segmentation holds a significant place. This process involves distinguishing pixels of organs or lesions in medical images, such as CT scans [9] and Endoscopy [20] videos. Medical image segmentation is one of the most difficult tasks in medical image analysis, with the goal of providing and extracting vital information regarding the shape and volume of these organs or tissues. Deep learning techniques have been used recently to improve medical image segmentation. These models extract useful information from images, increase accuracy, and adapt to different datasets and tasks.

A common approach for semantic image segmentation is the use of an Encoder-Decoder network with skip connections. In this framework, the Encoder captures hierarchical and abstract features from an input image. The Decoder, on the other hand, uses the feature maps produced by the Encoder to build a pixel-wise segmentation mask or map, attributing a class label to each pixel in the input image. Numerous studies have been done to integrate global information into feature maps and enhance multi-scale features, leading to significant enhancements in segmentation performance [4,26,12,5,22].

U-Net [16] is a pivotal architecture celebrated for its balanced Encoder-Decoder design and the incorporation of skip connections. This structure allows for the extraction of feature information at multiple levels through its various encoders and decoders. Furthermore, skip connections facilitate the effective transition of this feature information. Numerous studies on U-Net primarily focus on the following aspects: Encoder section - Different backbones are replaced to obtain feature maps of varying levels [22]; Skip connections - Various channel attention mechanisms are adopted, and different connection parts are interchanged [15]; Decoder section - Different sampling and feature fusion schemes are used [23,25].

CNN-based models, due to their local receptive field, struggle to capture long-range information, which can lead to poor feature extraction and sub-optimal segmentation results. Transformer-based models excel in global modeling but their self-attention mechanism’s quadratic complexity creates high computational costs, especially in tasks like medical image segmentation that require dense predictions. These limitations necessitate a new architecture for medical image segmentation that can capture long-range information efficiently while maintaining linear computational complexity. Recent advancements in State Space Models (SSMs), particularly Structured SSMs (S4), provide an effective solution due to their proficiency in handling long sequences. e.g., Mamba [10]. The Mamba model augments S4 with a selective mechanism and hardware optimization, demonstrating outstanding performance in dense data domains. The incorporation of the Cross-Scan Module (CSM) in the Visual State Space Model (VMamba) [13] further boosts Mamba’s suitability for computer vision tasks. It does this by facilitating the traversal of the spatial domain and transforming non-causal visual images into ordered patch sequences.

Influenced by the success of VMamba [13] in image classification task and VM-Unet [17] in medical image segmentation. Following the framework of UNetV2 [15], this paper introduces the Vision Mamba UNetV2 (VM-UNetV2), we re-integrate low-level and high-level features, infusing semantic information into the low-level features, while using more detailed information to refine the high-level features.

We carry out exhaustive experiments on tasks related to gastroenterology semantic segmentation task and skin lesion segmentation to showcase the capabilities of pure SSM-based models in the field of medical image segmentation. In particular, we perform extensive testing on the ISIC17, ISIC18, CVC-300, CVC-ClinicDB, Kvasir, CVC-ColonDB and ETIS-LaribPolypDB public datasets and

ZD-LCI-EGGIM our private dataset. The outcomes suggest that VM-UNetV2 can deliver competitive results.

The primary contributions of this study can be encapsulated in the following points: 1) We proposed VM-UnetV2, We have pioneered the exploration of better SSM-based algorithms in medical image segmentation. 2) Exhaustive experiments are performed on seven datasets, with outcomes demonstrating that VM-UNetV2 showcases significant competitiveness. 3) We are pioneering the exploration of combining SSM-based with Unet variants, driving the development of more efficient and effective SSM-based segmentation algorithms.

The rest of the paper is organized as follows: Sec.2 introduces the algorithm design consideration. Sec.3 presents the experiments details and results. Sec.4 concludes the paper.

2 Methods

2.1 Preliminaries

In contemporary SSM-based models, namely, Structured State Space Sequence Models (S4) and Mamba [10,13,17], both depend on a traditional continuous system that maps a one-dimensional input function or sequence, represented as $x(t) \in R$, through intermediary implicit states $h(t) \in R^N$ to an output $y(t) \in R$. This process can be depicted as a linear Ordinary Differential Equation (ODE):

$$\begin{aligned} h'(t) &= Ah(t) + Bx(t) \\ y(t) &= Ch(t) \end{aligned} \tag{1}$$

where $\mathbf{A} \in R^{N \times N}$ represents the state matrix, while $\mathbf{B} \in R^{N \times 1}$ and $\mathbf{C} \in R^{N \times 1}$ denote the projection parameters.

S4 and Mamba discretize this continuous system to adapt it better for deep learning contexts. Specifically, they incorporate a timescale parameter Δ and convert \mathbf{A} and \mathbf{B} into discrete parameters $\overline{\mathbf{A}}$ and $\overline{\mathbf{B}}$ using a consistent discretization rule. The zero-order hold (ZOH) is typically utilized as the discretization rule and can be outlined as follows:

$$\begin{aligned} \overline{\mathbf{A}} &= \exp(\Delta \mathbf{A}) \\ \overline{\mathbf{B}} &= (\Delta \mathbf{A})^{-1}(\exp(\Delta \mathbf{A}) - \mathbf{I}) \cdot \Delta \mathbf{B} \end{aligned} \tag{2}$$

Following discretization, SSM-based models can be calculated in two distinct methods: linear recurrence or global convolution, which are denoted as equations (3) and (4), respectively.

$$\begin{aligned} h'(t) &= \overline{\mathbf{A}}h(t) + \overline{\mathbf{B}}x(t) \\ y(t) &= \mathbf{C}h(t) \end{aligned} \tag{3}$$

$$\begin{aligned} \bar{K} &= \left(\overline{C\mathbf{B}}, \overline{C\mathbf{A}\mathbf{B}}, \dots, \overline{C\mathbf{A}^{L-1}\mathbf{B}} \right) \\ y &= x * \bar{K} \end{aligned} \quad (4)$$

where $\bar{K} \in R^L$ represents a structured convolutional kernel, and L denotes the length of the input sequence x .

2.2 VM-UNetV2 Architecture

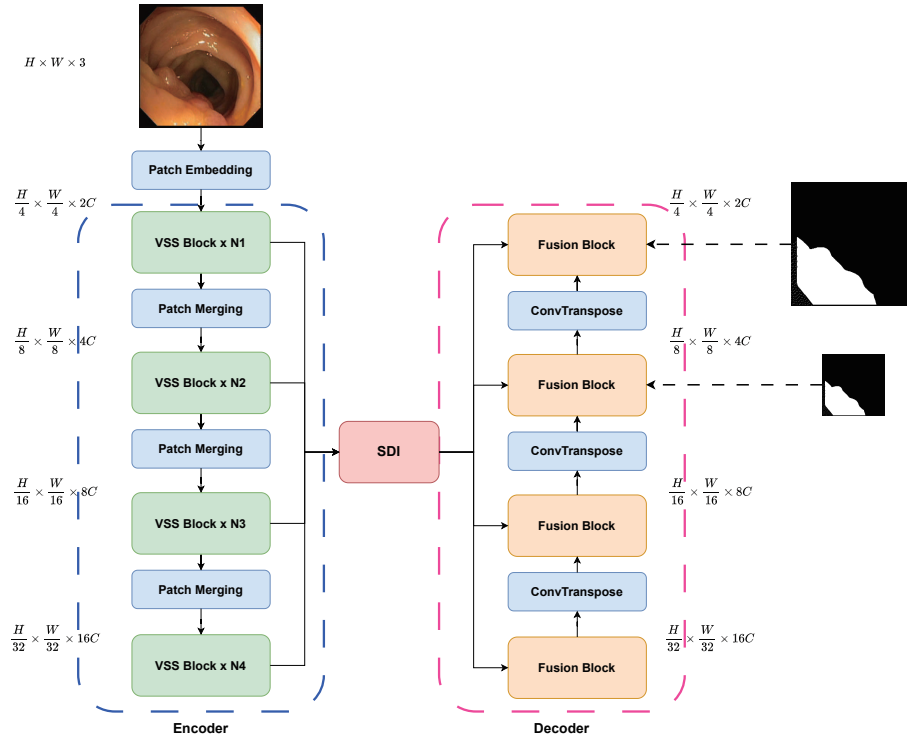


Fig. 1. The overall architecture of Vision Mamba UNetV2 model, which consists of an Encoder module, SDI(semantics and detail infusion) [15] module, and an Decoder module

The comprehensive structure of Vision Mamba UNetV2 is depicted in Fig 1. It consists of three primary modules: the Encoder, the SDI (Semantic and Detail Infusion) [15] module, and the Decoder. Given an input image I , where $I \in R^{H \times W \times 3}$, the encoder generates features at M levels. We represent the features

at the i_{th} level as f_i^o , where $1 \leq i \leq M$. These accumulated features, $\{f_1^o, f_2^o, \dots, f_M^o\}$ are subsequently forwarded to the SDI module for further enhancement.

As described the Figure, the Encoder output channel of f_i is $2^i \times C$, $\{f_1^o, f_2^o, \dots, f_M^o\}$ collectively enter the SDI module for feature fusion, and f_i corresponds to f_i' as the output of the i_{th} stage. The feature of f_i' is $\frac{H}{2^{i+1}} \times \frac{W}{2^{i+1}} \times 2^i C$. In our model, we use deep supervision to calculate the loss of f_i' and f_{i-1}' features.

In this paper, we employ $[N_1, N_2, N_3, N_4]$ VSS blocks across Encoder four stages, with the channel counts for each stage being $[C, 2C, 4C, 8C]$. From our observations in VMamba [13], the different values of N_3 and c are important factors that distinguish between Tiny, Small, and Base framework specs. Following the specifications of VMamba, we let C take the value of 96, N_1 and N_2 each take the value of 2, and N_3 take values from the set $[2, 9, 27]$. This represents our intention to use the Tiny and Small models of VMamba as the backbone for our ablation experiments.

2.3 VSS And SDI Block

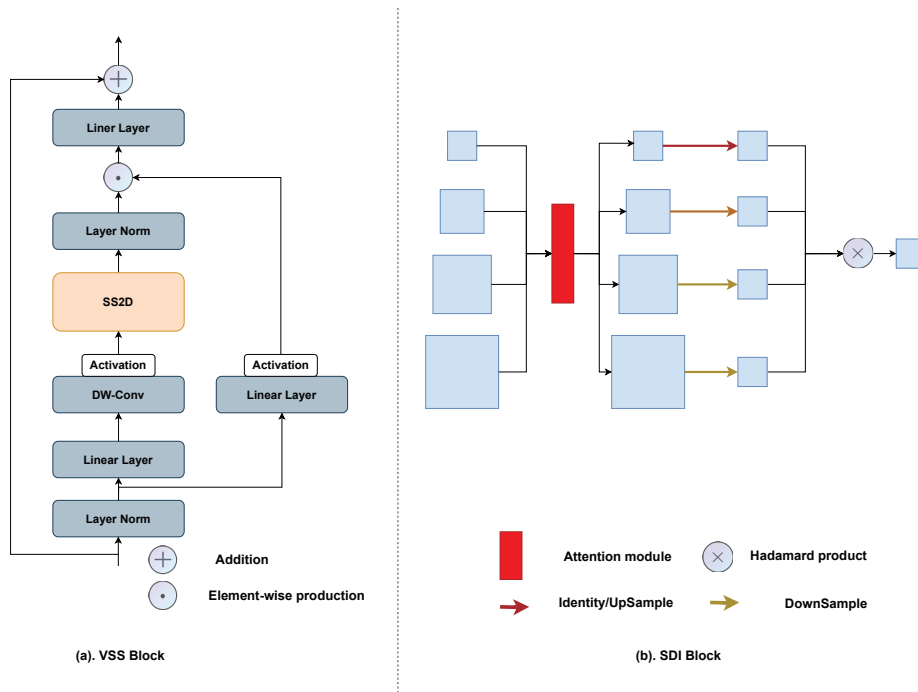


Fig. 2. a. VSS Block as the backbone of VMUNetV2, and the SS2D is the core of VSS block b. (Semantics and Detail Infusion)SDI module consists of backbone’s output features, an Attention module, output features of SDI are with the different size the same as backbone’s output features.

The VSS block derived from VMamba, As the backbone part of the VM-UNetV2 Encoder, The structure of VSS block is illustrated in Figure 2(a). The input is first processed through an initial linear embedding layer, after which it divides into two separate information streams. One stream is directed through a 3×3 depth-wise convolution [11] layer and subsequently a Silu activation [19] function before it enters the main 2D-Selective-Scan(SS2D) module. The SS2D output then proceeds through a layer normalization layer and is combined with the output from the other information stream, which has also been processed through a Siluactivation. This merged output constitutes the final result of the VSS block.

The SDI module [15], As described in Figure 2 (b). With the hierarchical feature maps $f_i^0 = \frac{H}{2^{i+1}} \times \frac{W}{2^{i+1}} \times 2^i C, 1 \leq i \leq 4$ generated by the encoder, where i represents the i_{th} level.

Different Attention mechanisms can be used in the SDI module to calculate the attention scores for both space and channel. Following what is mentioned in UNetV2 [15], we use CBAM [22] to implement spatial and temporal attention. The calculation formula is as follows, and ϕ_i^{att} represents the i_{th} attention calculation:

$$f_i^1 = \phi_i^{att} (f_i^0) \quad (5)$$

Then we use 1×1 convolution to align the channel of f_i^1 to c the resulted feature map is denoted as $f_i^2 \in R^{H_i \times W_i \times c}$.

In SDI decoder i_{th} stage, f_i^2 denotes target reference. Then we adjust the sizes of the feature maps at every j_{th} level to match the size of f_i^2 , as formulated below:

$$f_{ij}^3 = \begin{cases} G_d (f_j^2, (H_i, W_i)) & \text{if } j < i, \\ G_i (f_j^2) & \text{if } j = i, \\ G_u (f_j^2, (H_i, W_i)) & \text{if } j > i, \end{cases} \quad (6)$$

In the formula 6, G_d , G_i and G_u represent adaptive average pooling, identity mapping, and bilinearly interpolating. In the formula 7, θ_{ij} represents the parameters of the smooth convolution, and f_{ij}^4 is the j_{th} smoothed feature map at the i_{th} level. Here, H () represents the Hadamard product. Subsequently, f_i^5 is forwarded to the decoder at the i_{th} level for further reconstruction of resolution and segmentation.

$$\begin{aligned} f_{ij}^4 &= \theta_{ij} (f_{ij}^3) \\ f_i^5 &= H ([f_{i1}^4, f_{i2}^4, f_{i3}^4, f_{i4}^4]) \end{aligned} \quad (7)$$

2.4 Loss function

For our medical image segmentation tasks, we primarily employ basic Cross-Entropy and Dice loss as the loss function cause all of our dataset masks comprise two classes, which are a singular target and the background.

$$\begin{aligned}
L_{BceDice} &= \lambda_1 L_{Bce} + \lambda_2 L_{Dice} \\
L_{Bce} &= -\frac{1}{N} \sum_1^N [y_i \log(\hat{y}_i) + (1 - y_i) \log(1 - \hat{y}_i)] \\
L_{Dice} &= 1 - \frac{2|X \cap Y|}{|X| + |Y|}
\end{aligned} \tag{8}$$

(λ_1, λ_2) are constants, with $(1, 1)$ often selected as the default parameters.

3 Experiments and results

3.1 Datasets

We use three types of datasets to verify the effectiveness of our framework. The first type is the open-source skin diseases dataset, including ISIC 2017 and ISIC 2018, we split the skin datasets in a 7: 3 ratio for use as training and testing sets. The second is the open-source gastrointestinal polyp dataset, which includes Kvasir-SEG, ClinicDB, ColonDB, Endoscene, and ETIS, in this type datasets we follow the experimental setups in PraNet. For these datasets, we provide detailed evaluations on several metrics, including Mean Intersection over Union(mIoU), Dice Similarity Coefficient(DSC), Accuracy(Acc), Sensitivity(Sen), and Specificity(Spe).

3.2 Experimental setup

Following the VMamba work, we adjust the image dimensions in all datasets to 256×256 pixels. With the aim of curbing overfitting, we also bring in data augmentation methods, such as random flipping and random rotation. In terms of operational parameters, we have the batch size set at 80, with the AdamW optimizer engaged starting with a learning rate of 1e-3. We make use of CosineAnnealingLR as the scheduler, with its operation spanning a maximum of 50 iterations and the learning rate going as low as 1e-5. We conduct our training over the course of 300 epochs. For the VM-UNetV2, the encoder units' weights are initially set to align with those of VMamba-S. The implementation was carried out on an Ubuntu 20.04 system, using Python3.9.12, PyTorch2.0.1, and CUDA11.7. All experiments are conducted on a single NVIDIA RTX V100 GPU.

3.3 Results

We compare VM-UNetV2 with some state-of-the-art models, presenting the experimental results in Table 1 and Table 2. For the ISIC datasets, our VM-UNetV2 outperforms other models in terms of the mIoU, DSC and Acc metrics. In the polyp-related datasets, our model also surpasses the state-of-the-art model UNetV2 in all metrics, with an increase of up to 7% in the mIoU parameter.

Table 1. Comparative experimental results on the ISIC17 and ISIC18 datasets(Bold indicates the best)

Dataset	Model	mIoU(%) \uparrow	DSC(%) \uparrow	Acc(%) \uparrow	Spe(%) \uparrow	Sen(%) \uparrow
ISIC17	UNet [16]	76.98	86.99	95.65	97.43	86.82
	UTNetV2 [8]	77.35	87.23	95.84	98.05	84.85
	TransFuse [24]	79.21	88.40	96.17	97.98	87.14
	MALUNet [18]	78.78	88.13	96.18	98.47	84.78
	UNetV2 [15]	82.18	90.22	96.78	98.40	88.71
	VM-UNet [17]	80.23	89.03	96.29	97.58	89.90
	VM-UNetV2	82.34	90.31	96.70	97.67	91.89
ISIC18	UNet [16]	77.86	87.55	94.05	96.69	85.86
	UNet++ [26]	78.31	87.83	94.02	95.75	88.65
	Att-Unet [14]	78.43	87.91	94.13	96.23	87.60
	UTNetV2 [8]	78.97	88.25	94.32	96.48	87.60
	SANet [21]	79.52	88.59	94.39	95.97	89.46
	TransFuse [24]	80.63	89.27	94.66	95.74	91.28
	MALUNet [18]	80.25	89.04	94.62	96.19	89.74
	UNetV2 [15]	80.71	89.32	94.86	96.94	88.34
	VM-UNet [17]	81.35	89.71	94.91	96.13	91.12
	VM-UNetV2	81.37	89.73	95.06	97.13	88.64

Table 2. Comparative experimental results on the Kvasir-SEG, ClinicDB, ColonDB, ETIS and CVC-300 datasets(Bold indicates the best)

Dataset	Model	mIoU(%) \uparrow	DSC(%) \uparrow	Acc(%) \uparrow	Spe(%) \uparrow	Sen(%) \uparrow
Kvasir-SEG	UNetV2	84.00	91.30	97.47	99.08	88.39
	VMUnet	80.32	89.09	96.80	98.49	87.21
	VMUnetV2	84.15	91.34	97.52	99.25	87.71
ClinicDB	UNetV2	83.85	91.21	98.59	99.16	91.99
	VMUnet	81.95	90.08	98.42	99.18	89.73
	VMUnetV2	89.31	94.35	99.09	99.38	95.64
ColonDB	UNetV2	57.29	72.85	96.19	98.43	68.46
	VMUnet	55.28	71.20	96.02	98.45	65.89
	VMUnetV2	60.98	75.76	96.54	98.46	72.68
ETIS	UNetV2	71.90	83.65	98.35	98.61	92.96
	VMUnet	66.41	79.81	98.26	99.33	75.79
	VMUnetV2	72.29	83.92	98.47	98.96	88.07
CVC-300	UNetV2	82.86	90.63	99.34	99.54	93.82
	VMUnet	79.55	88.61	99.20	99.44	92.46
	VMUnetV2	89.31	94.35	99.08	99.38	95.64

Beyond evaluating the accuracy of the models, we also assess the computational complexity of different models, leveraging the advantage of VMamba’s linear complexity. We use metrics such as model inference speed FPS (frames per second), model parameter count (Params), and the number of floating point operations (FLOPs) for this evaluation, as depicted in Table 3. (3, 256, 256) represents the size of the input image. All the tests are conducted on an NVIDIA V100 GPU. the FLOPs and FPS of VM-UNetV2 are superior to those of others.

Table 3. Comparison of computational complexity, GPU memory usage, and inference time, using an NVIDIA V100 GPU(Bold indicates the best).

Model	Input size	Params(M)↓	FLOPs(G)↓	FPS↑
UNetV2	(3, 256, 256)	25.15	5.40	32.74
VM-Unet	(3, 256, 256)	34.62	7.56	20.612
VM-UnetV2	(3, 256, 256)	17.91	4.40	32.58

3.4 Ablation studies

In this section, we conduct ablation experiments on the initialization of VM-UNetV2 Encoder and the Deep Supervision operation of Decoder using the polyp datasets. As stated in the VMamba [13] paper, the depth of the Encoder and the number of channels in the feature map determine the scale of VMamba. In this paper, the proposed VM-UNetV2 only uses the pre-trained weights of VMamba on ImageNet-1k for the Encoder part. Therefore, when conducting the model scale ablation experiment in this study, we only vary the depth of the Encoder, as shown in the Table 4. For the output features, we employ a Deep Supervision mechanism, using a fusion of two layers of output features, which are then compared with the real labels for loss computation.

As shown in Table 4 and Table 5, when the depth of the Encoder is set to [2, 2, 9, 2], the segmentation evaluation metrics are relatively better. Therefore, when using VM-UNetV2, there is no need to choose a particularly large depth. In most cases where the Deep Supervision mechanism is used, the segmentation evaluation metrics are relatively better, but it is not a decisive factor. For different datasets, ablation experiments need to be conducted separately to determine whether to adopt the Deep Supervision mechanism.

4 Conclusions

In this paper, we propose a SSM-based UNet type medical image segmentation model, VM-UNetV2, which fully utilizes the capabilities of SSM-based models. We use VSS blocks and SDI to process the Encoder and Skip connection, respectively. The pre-trained weights of VMamba are used to initialize the Encoder part of VM-UNetV2, and a Deep Supervision mechanism is employed

Table 4. Ablation studies on Encoder Depth and Deep Supervision of VM-UNet-V2 (part 1)

Encoder Depth	Deep Supervision	Kvasir-SEG		ClinicDB	
		mIoU(%)↑	DSC(%)↑	mIoU(%)↑	DSC(%)↑
[2,2,2,2]	TRUE	82.93	90.67	83.08	90.76
	FALSE	82.59	90.47	85.40	92.13
[2,2,9,2]	TRUE	85.23	92.03	89.02	94.19
	FALSE	84.15	91.39	89.31	94.35
[2,2,27,2]	TRUE	82.90	90.65	88.45	93.87
	FALSE	79.57	88.63	80.58	89.24

Table 5. Ablation studies on Encoder Depth and Deep Supervision of VM-UNet-V2 (part 2)

ColonDB		ETIS		CVC-300	
mIoU(%)↑	DSC(%)↑	mIoU(%)↑	DSC(%)↑	mIoU(%)↑	DSC(%)↑
57.68	73.16	66.22	79.68	76.50	86.68
54.44	70.5	68.05	80.98	77.66	87.42
62.94	77.26	67.94	80.91	80.43	89.15
60.98	75.76	72.29	83.92	79.23	88.41
64.06	78.09	70.72	82.85	80.32	89.09
57.03	72.63	63.55	77.72	77.66	87.42

to supervise multiple output features. Our model has been extensively tested on skin disease and polyp datasets. The results demonstrate that our model is highly competitive in segmentation tasks. Complexity analysis suggested that VM-UNetV2 is also efficient in FLOPs, Params and FPS.

References

1. Alom, M.Z., Yakopcic, C., Hasan, M., Taha, T.M., Asari, V.K.: Recurrent residual u-net for medical image segmentation. *Journal of Medical Imaging* **6**(1), 014006–014006 (2019)
2. Azad, R., Al-Antary, M.T., Heidari, M., Merhof, D.: Transnorm: Transformer provides a strong spatial normalization mechanism for a deep segmentation model. *IEEE Access* **10**, 108205–108215 (2022)
3. Azad, R., Heidari, M., Shariatnia, M., Aghdam, E.K., Karimijafarbigloo, S., Adeli, E., Merhof, D.: Transdeeplab: Convolution-free transformer-based deeplab v3+ for medical image segmentation. In: *International Workshop on PRedictive Intelligence In MEDicine*. pp. 91–102. Springer (2022)
4. Chen, J., Lu, Y., Yu, Q., Luo, X., Adeli, E., Wang, Y., Lu, L., Yuille, A.L., Zhou, Y.: Transunet: Transformers make strong encoders for medical image segmentation. *arXiv preprint arXiv:2102.04306* (2021)
5. Chen, L.C., Zhu, Y., Papandreou, G., Schroff, F., Adam, H.: Encoder-decoder with atrous separable convolution for semantic image segmentation. In: *Proceedings of the European conference on computer vision (ECCV)*. pp. 801–818 (2018)

6. Cheng, J.Z., Ni, D., Chou, Y.H., Qin, J., Tiu, C.M., Chang, Y.C., Huang, C.S., Shen, D., Chen, C.M.: Computer-aided diagnosis with deep learning architecture: applications to breast lesions in us images and pulmonary nodules in ct scans. *Scientific reports* **6**(1), 24454 (2016)
7. Çiçek, Ö., Abdulkadir, A., Lienkamp, S.S., Brox, T., Ronneberger, O.: 3d u-net: learning dense volumetric segmentation from sparse annotation. In: *Medical Image Computing and Computer-Assisted Intervention–MICCAI 2016: 19th International Conference, Athens, Greece, October 17–21, 2016, Proceedings, Part II* 19. pp. 424–432. Springer (2016)
8. Gao, Y., Zhou, M., Liu, D., Metaxas, D.: A multi-scale transformer for medical image segmentation: Architectures, model efficiency, and benchmarks. *arXiv preprint arXiv:2203.00131* (2022)
9. Golan, R., Jacob, C., Denzinger, J.: Lung nodule detection in ct images using deep convolutional neural networks. In: *2016 international joint conference on neural networks (IJCNN)*. pp. 243–250. IEEE (2016)
10. Gu, A., Dao, T.: Mamba: Linear-time sequence modeling with selective state spaces. *arXiv preprint arXiv:2312.00752* (2023)
11. Howard, A.G., Zhu, M., Chen, B., Kalenichenko, D., Wang, W., Weyand, T., Andreetto, M., Adam, H.: Mobilenets: Efficient convolutional neural networks for mobile vision applications. *arXiv preprint arXiv:1704.04861* (2017)
12. Liu, S., Qi, L., Qin, H., Shi, J., Jia, J.: Path aggregation network for instance segmentation. In: *Proceedings of the IEEE conference on computer vision and pattern recognition*. pp. 8759–8768 (2018)
13. Liu, Y., Tian, Y., Zhao, Y., Yu, H., Xie, L., Wang, Y., Ye, Q., Liu, Y.: Vmamba: Visual state space model. *arXiv preprint arXiv:2401.10166* (2024)
14. Oktay, O., Schlemper, J., Folgoc, L.L., Lee, M., Heinrich, M., Misawa, K., Mori, K., McDonagh, S., Hammerla, N.Y., Kainz, B., et al.: Attention u-net: Learning where to look for the pancreas. *arXiv preprint arXiv:1804.03999* (2018)
15. Peng, Y., Sonka, M., Chen, D.Z.: U-net v2: Rethinking the skip connections of u-net for medical image segmentation. *arXiv preprint arXiv:2311.17791* (2023)
16. Ronneberger, O., Fischer, P., Brox, T.: U-net: Convolutional networks for biomedical image segmentation. In: *Medical Image Computing and Computer-Assisted Intervention–MICCAI 2015: 18th International Conference, Munich, Germany, October 5–9, 2015, Proceedings, Part III* 18. pp. 234–241. Springer (2015)
17. Ruan, J., Xiang, S.: Vm-unet: Vision mamba unet for medical image segmentation. *arXiv preprint arXiv:2402.02491* (2024)
18. Ruan, J., Xiang, S., Xie, M., Liu, T., Fu, Y.: Malunet: A multi-attention and light-weight unet for skin lesion segmentation. In: *2022 IEEE International Conference on Bioinformatics and Biomedicine (BIBM)*. pp. 1150–1156. IEEE (2022)
19. Shazeer, N.: Glu variants improve transformer. *arXiv preprint arXiv:2002.05202* (2020)
20. Tang, D., Wang, L., Ling, T., Lv, Y., Ni, M., Zhan, Q., Fu, Y., Zhuang, D., Guo, H., Dou, X., et al.: Development and validation of a real-time artificial intelligence-assisted system for detecting early gastric cancer: A multicentre retrospective diagnostic study. *EBioMedicine* **62** (2020)
21. Wei, J., Hu, Y., Zhang, R., Li, Z., Zhou, S.K., Cui, S.: Shallow attention network for polyp segmentation. In: *Medical Image Computing and Computer Assisted Intervention–MICCAI 2021: 24th International Conference, Strasbourg, France, September 27–October 1, 2021, Proceedings, Part I* 24. pp. 699–708. Springer (2021)

22. Woo, S., Park, J., Lee, J.Y., Kweon, I.S.: Cbam: Convolutional block attention module. In: Proceedings of the European conference on computer vision (ECCV). pp. 3–19 (2018)
23. Yu, F., Koltun, V.: Multi-scale context aggregation by dilated convolutions. arXiv preprint arXiv:1511.07122 (2015)
24. Zhang, Y., Liu, H., Hu, Q.: Transfuse: Fusing transformers and cnns for medical image segmentation. In: Medical Image Computing and Computer Assisted Intervention–MICCAI 2021: 24th International Conference, Strasbourg, France, September 27–October 1, 2021, Proceedings, Part I 24. pp. 14–24. Springer (2021)
25. Zhou, X.Y., Zheng, J.Q., Li, P., Yang, G.Z.: Acnn: a full resolution dcnn for medical image segmentation. In: 2020 IEEE International Conference on Robotics and Automation (ICRA). pp. 8455–8461. IEEE (2020)
26. Zhou, Z., Rahman Siddiquee, M.M., Tajbakhsh, N., Liang, J.: Unet++: A nested u-net architecture for medical image segmentation. In: Deep Learning in Medical Image Analysis and Multimodal Learning for Clinical Decision Support: 4th International Workshop, DLMIA 2018, and 8th International Workshop, ML-CDS 2018, Held in Conjunction with MICCAI 2018, Granada, Spain, September 20, 2018, Proceedings 4. pp. 3–11. Springer (2018)